Comparison of Flexural Stiffness between Hat-type and U-type Steel Sheet Pile Retaining Walls in a Field Test in Singapore

S. Moriyasu[1], S.P. Chiew[2], K. Otsushi[3], N. Matsui[4], S. Taenaka[5], K. Teshima[6], M. Tatsuta[7] and H. Tanaka[8]
[1,5]*Steel Structures Research Lab, Nippon Steel Corporation, Chiba, Japan*
[2]*Singapore Institute of Technology, Singapore*
[3]*Nippon Steel South East Asia Pte Ltd, Singapore, Singapore*
[4,6,7,8]*Construction Products Development Div., Nippon Steel Corporation, Tokyo, Japan*
[1]*E-mail:* moriyasu.45e.shunsuke@jp.nipponsteel.com
[2]*E-mail:* singping.chiew@singaporetech.edu.sg
[3]*E-mail:* otsushi.k78.kazutaka@sg.nipponsteel.com
[4]*E-mail:* matsui.c4d.nobuyuki@jp.nipponsteel.com

ABSTRACT: The use of the Hat-type steel sheet pile can potentially improve the performance of earth retaining walls because of two of its features: its wide width and location of interlocks. It can reduce the piling time and number of piles required for walls because of its 900-mm width, which is the widest among the hot-rolled monopiles in the world. Furthermore, Hat-type piles can achieve full-shear force transmission at the interlocks because their connections are located at the outer edge of the wall. This study focuses on the second feature, i.e., the interlock shear force transmission. The lateral load and excavation tests were performed to compare and verify the difference in the interlock behavior between U-type and Hat-type sheet piles. As the result, in contract to the reduction of shear force transmission of the U-pile wall, the Hat-pile wall exhibited high flexural stiffness because the interlocks achieved the full-shear transmission mode.

KEYWORDS: Steel Sheet Pile, Retaining Wall, Interlock Shear Force Transmission, Lateral Load Test, Excavation Test

1. INTRODUCTION

In recent years, construction works for public facilities, including roads, railways, and ports, have flourished in Southeast Asian countries with high economic growth, such as Singapore, Indonesia, and Vietnam. In these ASEAN countries, it has been expected that more effective construction technologies would improve productivity.

The erection of earth retaining walls is one of the main construction works for public facilities. Retaining walls are employed in temporary and permanent structures, securing excavations, waterfront structures, revetments, quay walls, bridge abutments, and so on. The steel sheet pile wall, as the main type of earth retaining wall, can function similar to a concrete structure. As a pile wall, the advantage of steel is its high material reliability, excellent homogeneity, high recyclability, and reusability. However, the U-shaped steel sheet pile (U pile), which is a widely used pile in the world, exhibits a structural problem as an earth retaining wall. Because the interlocks of the U-pile wall are located at the center of the wall, the shear force related to the bending force loses its transmission between interlocks. As a result, the interlocks slip, and the flexural stiffness of the wall is reduced. According to EN 1993-5, UK National Annex to Eurocode 3 and Singapore National Annex to Eurocode 3, the moment of inertia and section modulus of the U-pile wall should be reduced according to the soil condition, interlock crimp condition, and number of struts. Konoike (1986) and Endley (1991) conducted field tests to investigate the reduction of flexural stiffness because of the insufficiency of the shear force transmission in the U-pile wall. Shiraishi (1987) suggested a method to evaluate the degree of this insufficiency of shear force transmission. Byfield (2004) studied the influence of soil inside the interlock on the flexural stiffness of the U-pile wall by means of a structural test. Overall, these studies show that the dearth of the shear force transmission in U-pile walls is a fundamental problem.

The hat-shaped steel sheet pile (Hat pile), described in JIS A 5233, can possibly solve this problem. Figure 1 shows a comparison of the shape of a Hat pile to that of a U pile. The 900-mm effective width of a Hat pile is greater than the width of a double U pile. Here, the effective width means each pile width considering the overlapped width of connected interlocks. It is also the widest hot-rolled pile in the world. Hence, Hat piles can be used to construct a pile wall with fewer piles and shorter piling times compared to the use of U-piles. Furthermore, the interlocks of Hat piles are located on the outermost edge of the pile wall. As shown in Figure 2, the location of these interlocks corresponds to a small shear stress zone, whereas that of a U-pile wall corresponds to a large shear stress zone. Thus, the flexural stiffness of the Hat-pile wall is not reduced because of insufficient shear force transmission. Consequently, the use of Hat piles could potentially improve productivity, construction technology, and economic efficiency. In the case of Japan, Harata (2008) and Otsushi (2016) mentioned that Hat piles are regarded as materials superior to U piles and widely used to improve productivity.

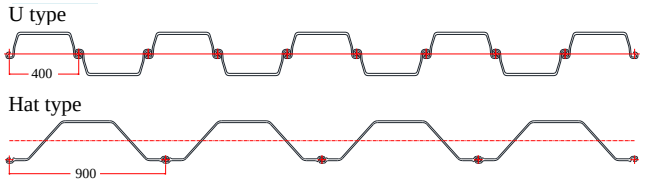

Figure 1 Overview of U and Hat-pile walls

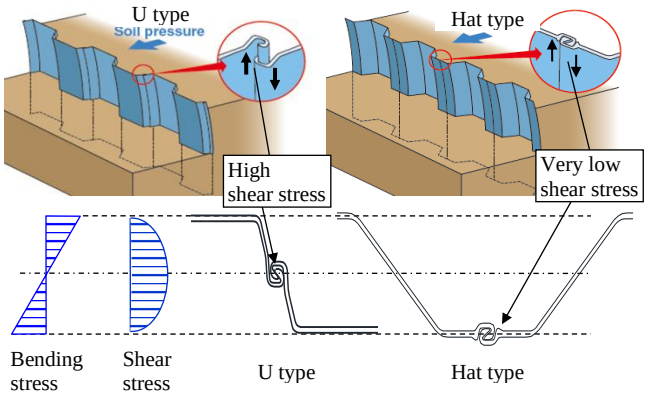

Figure 2 Positional relationship between the interlock of two types of piles and shear force distribution on pile walls

In order to verify the differences in the interlock shear force transmission and flexural stiffness between Hat and U-pile walls, a series of field tests, involving the lateral load test and excavation test, was performed in Singapore. This paper presents the results of the field tests and discusses the difference in the structural performance between the Hat-pile and U-pile walls in terms of the interlock shear force transmission.

2. OUTLINE OF THE FIELD TEST

2.1 Test content and procedure

In a series of tests, a lateral load test and an excavation test were performed. Table 1 lists the test cases, and Figure 3 shows the pile locations and tests involved. First, two cases of the lateral load tests were conducted: 25H-pile and IV-pile walls in Case 1, and 45H-pile and IV-pile walls in Case 2. Then, to construct a cofferdam during the excavation test, the piles used in Case 1 were extracted, and their upsides were cut to eliminate the bent portion caused by the lateral load tests. Thereafter, the piles were reinstalled next to the walls of Case 2. The sidewalls of the cofferdam consisted of Hat piles. Finally, for the excavation test, the inside of the cofferdam was dug.

Table 1 Test cases

Test	Case	Type	Name	Pile Length L (m)	Wall width W (m)
Lateral load test	1	25H	25H-L16.5 pile	16.5	3.6 [4 pcs]
		IV	IV-L16.5 pile	16.5	3.2 [8 pcs]
	2	45H	45H-L15.5 pile	15.5	3.6 [4 pcs]
		IV	IV-L15.5 pile	15.5	3.2 [8 pcs]
Excavation test	3	25H	25H-L12 pile	12.0	3.6 [4 pcs]
		IV	IV-L12 pile	12.0	3.2 [8 pcs]
	4	45H	45H-L15.5 pile	15.5	3.6 [4 pcs]
		IV	IV-L15.5 pile	15.5	3.2 [8 pcs]

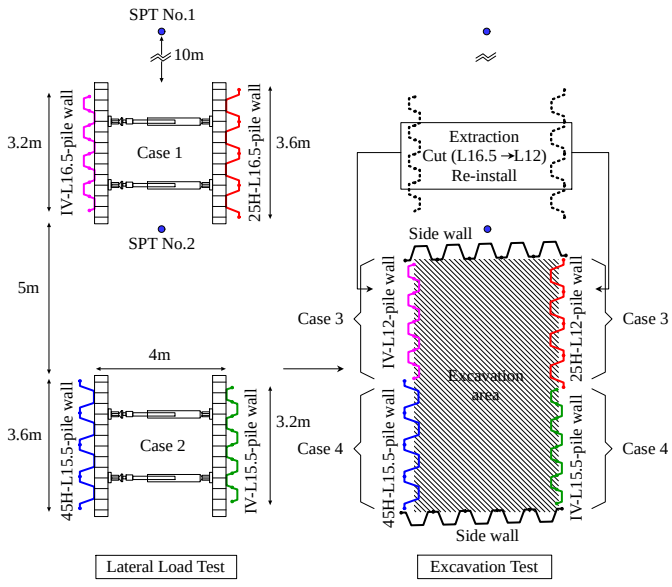

Figure 3 Pile location and test

2.2 Properties of the test piles

Table 2 summarizes the mechanical properties of the steel-sheet piles used in the test. In the table, 25H and 45H are the types of Hat piles, whereas IV is the type of the U piles. All materials are certified SYW 295 of JIS A 5233 (i.e., weldable hot-rolled steel sheet piles with yield stress, σ_y, exceeding 295 MPa). Here, JIS A 5233 is listed in Building and Construction Authority (2012) as one of the applicable steel materials in Singapore.

Table 2 Mechanical properties of steel sheet piles

		JIS A 5523		Mill certificate	
Type	Designation	Yield Stress σ_y (N/mm^2)	Tensile Stress σ_u (N/mm^2)	Yield Stress σ_{cy} (N/mm^2)	Tensile Stress σ_{cu} (N/mm^2)
25H	SYW295	295	450	374	498
45H	SYW295	295	450	380	490
IV	SYW295	295	450	370	537

Table 3 lists the dimensional properties of the aforementioned piles. The effective width of 25H and 45H is more than twice that of type IV pile. Both Hat piles can reduce the unit mass per meter width of pile wall because their thicknesses are less than that of the type IV pile. The test specimens are shown in Figure 4, and Table 4 summarizes the sectional properties per meter width of pile wall. It should be noted that the moment of inertia, I, and section modulus, Z, are not included in considering the inefficiency of the shear force transmission. When used in actual situations, I and Z of type IV pile may be reduced but should be verified in the test.

Table 3 Dimensional properties of steel sheet piles

Type	Effective width W_e (mm)	Effective height h_e (mm)	Thickness t (mm)	Sectional area A_s (cm^2)	Unit mass per pile length m (kg/m)
25H	900	300	13.2	144.4	113
45H	900	368	15.0	187.0	147
IV	400	170	15.5	96.99	76.1

Figure 4 Test piles (Left: Hat-45H-pile, Right: IV-pile)

Table 4 Sectional properties per meter width of pile wall

Type	Moment of inertia I (cm^4/m)	Section modulus Z (cm^3/m)
25H	24,400	1,610
45H	45,000	2,450
IV	38,600*	2,270*

*The lack of shear force transmission is not included

2.3 Soil conditions

The field test site corresponds to reclaimed land located on the coastal part of the southwest area in Singapore. Figure 5 shows the result of the soil investigation with the pile embedment length, L_e. Two standard penetration tests (SPTs) were conducted at the location marked in Figure 3. As shown on the left side of Figure 5, based on SPTs, the surface is covered by a 1.7 m deep hard sandy silt fill layer with cobbles. Below the 1.7-m depth, is relatively stiff filled silt, having penetration resistance (N) values of 7–20, exists. Soft silt, classified as Kallang formation, having N values of 0–6 exists below a depth of 4.8 m, and a soft to firm sandy silt layer, classified as Juroung formation, having N values of 4–20 exists below a depth of 8.9 m. The ground water table was detected at a depth of 1.1 m below the ground surface. The soil classification shown in Figure 5 is the result of SPT No. 1 which is similar to SPT No. 2. For unconfined compression tests, undisturbed soil samples were collected at three depths of the borehole of SPT No. 2 using the hydraulic piston thin wall sampler. As shown in Figure 5, the ground surface was excavated and backfilled through the series of tests. Furthermore, the pile embedment length, L_e, differed in each case because of the field test condition. Each L_e was enough length to keep the pile tip stable (i.e., the pile tip was not moved or rotated). Details about each tests are explained in the following sections.

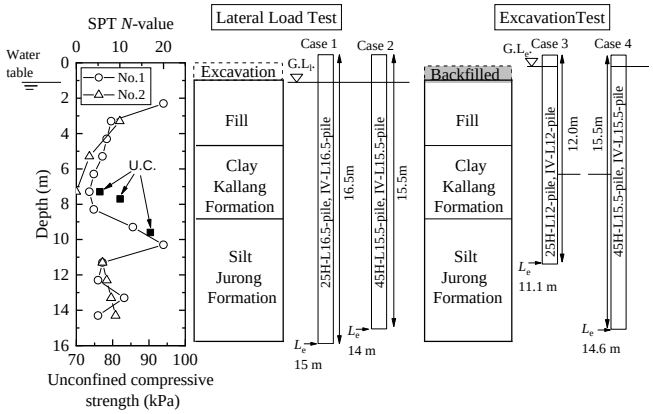

Figure 5 Soil conditions and pile embedment lengths

3. LATERAL LOAD TEST

3.1 Test conditions

As summarized in Table 1, the wall width, W, is not same among the cases. In Case 1, W = 3.6 m in the 25H-pile wall with four pieces of 25H-L16.5 piles, whereas W = 3.2 m in the IV-pile wall with eight pieces of IV piles. If nine pieces of IV-L16.5 piles were used, the IV-pile wall will have the same wall width as the 25H-pile wall (W = 3.6 m). However, the number pile pieces have to be adjusted to become even, because an uneven number of pile pieces shifts the neutral axis of the pile wall. As for the flexural stiffness of the wall, if the interlocks did not slip, the moment of inertia, I, of the IV-pile wall would be higher than that of the 25H-pile wall, although W of the former is shorter than that of the latter. As mentioned above, the purpose of the test is to investigate the actual flexural stiffness, including the interlock slippage.

Figure 6 illustrates the lateral load test setup. Two pile walls were constructed using a vibratory hammer (ICE-44B). The loading beams were placed on the brackets welded onto the surface of the piles. Two pieces of 1000-kN hydraulic jacks were set in parallel between the pile walls. The jack and loading beam were connected via the crevices. The two pile walls were pushed in opposite directions by the jacks.

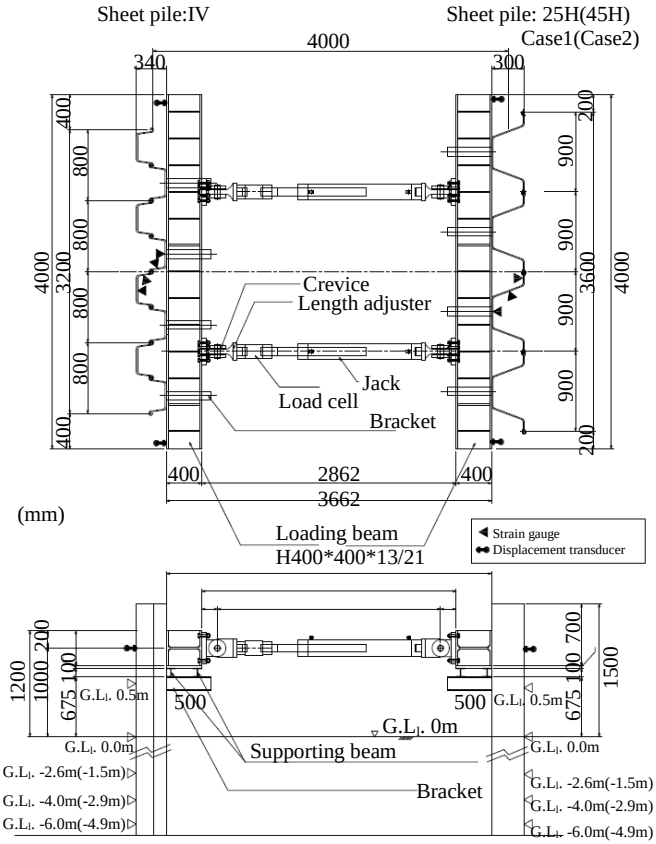

Figure 6 Lateral load test setup

The center of Figure 5 shows the relationship between the soil condition and pile embedment length, L_e. Before setting the piles, a 1-m deep excavation measured from the ground surface was made to remove the hard layer, including cobbles. Hence, the ground level in the lateral load test, $G.L_l$, was 1 m below from the original ground surface. As shown in Figure 5, L_e of the wall in Case 2 (L_e = 14.0 m) was made 1 m shallower than that of the wall in Case 1 (L_e = 15.0 m). The reason for this is to obtain the maximum bending strain in the depth direction. In Case 1, the maximum strain cannot be measured because of the gap between the levels of strain gauges and the actual generated maximum strain. Accordingly, in Case 2, L_e was adjusted to the level of the strain gauges after these had been attached to the piles.

The instrumentation of the test is shown in Figure 6. In order to obtain load–displacement curves, 1000-kN load cells were set between the jack heads and crevices. Moreover, displacement transducers were positioned at both edges of the loading beams at the same level with the jack loading point. Strain gauges were attached to measure the sectional strain distribution in the piles. As shown in Figure 6, the strain gauges were attached at five different levels. Details of the strain gauge measurement are explained in the next section.

3.2 Test results

3.2.1 Case1: 25H-pile wall and IV-pile wall

Figure 7 shows an overview of the test situation under the maximum load in Case 1. From the figure, the inclination of the IV-pile wall was larger than that of the 25H-pile wall. Additionally, as shown in Figure 8, the top portion of the IV-pile wall slipped by approximately 10 mm. Conversely, slippage was not observed on the 25H-pile wall, as shown in Figure 9.

Figure 7 Lateral load test at maximum load
(Case1: Left, IV-pile wall; Right, 25H-pile wall)

Figure 8 Interlock slippage at the top portion of the IV-pile wall

Figure 9 Top portion of the 25H-pile wall

These observations indicate that the flexural stiffness of the IV-pile wall decreased with the interlock slippage. Figure 10 shows the load–displacement curve of Case 1. The load is sum of the two load cell values. The vertical axis of Figure 10 was divided by the wall width, *W*, to consider the differences among the pile wall widths. Moreover, the displacement is the average of two measured deviations at points located at both edges of the loading beam. When the load reached 638 kN (200 kN/m for the IV-pile wall), the strain on the flange of the IV pile at G.L$_{l.}$ = 0.5 m reached the yield strain. Although the strain gauge may have been broken, the loading was completed because the difference in behavior between the 25H-pile wall and IV-pile wall was clearly observed. As shown in Figure 10, the gradient of the curve of the 25H-pile wall is equal to or greater than that of the IV-pile wall, although the moment of inertia, *I*, of the former is smaller than that of the latter without the interlock slippage. This indicates the actual flexural stiffness of the IV-pile wall decreased because of the lack of shear force transmission.

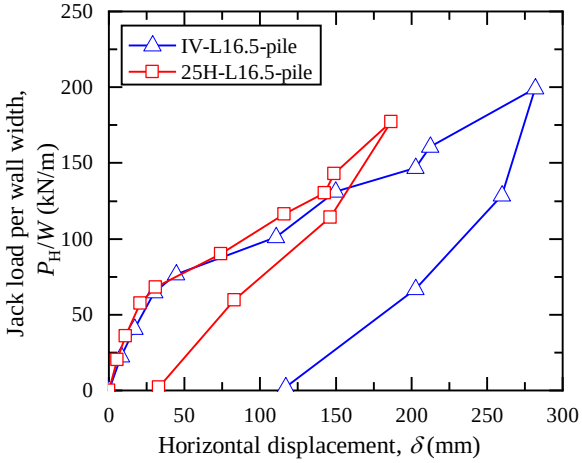

Figure 10 Relationship between the load per unit width of wall and displacement in Case 1

Figure 11 illustrates the locations of strain gauges in the pile section. In the case of the Hat-pile wall, strain gauges were attached to three segments of the pile per wall: the web, flange, and arm. Conversely, in the case of the IV-pile wall, the strain gauges were attached to two segments of two piles per wall: the web and flange. Furthermore, in Case 2, the strain gauges were set close to the interlock of the IV-pile wall at G.L$_{l.}$ = 0 m in order to obtain the section strain distribution in detail. Figures 12 and 13 show the strain distributions in the depth direction of each pile wall. The actual maximum strains in the depth direction may have been generated between G.L$_{l.}$ = 0 m and G.L$_{l.}$ = −2.6 m in both walls.

Hence, in order to obtain the actual maximum strains, the levels of strain gauges were changed in Case 2. In the 25H-pile wall, strains on the web and arm segments were considerably higher than that on the flange portion. Conversely, in the IV-pile wall, the strains on the flange segment, shown in Figure 12(d), considerably increased after the load exceeded 307 kN. Additionally, in Figure 12(b), the strain on the flange portion, at G.L$_{l.}$ = 6.0 m, was not measured because of the breakage of the strain gauge.

Figures 14 and 15 show the sectional strain distributions at each level. The strain distributions in the 25H-pile wall exhibit the behavior of a single wall, i.e., the maximum tensile and compressive strains were generated at the edge of the wall, and the neutral axis remained close to the center of the wall. In contrast, it is seen from Figure 15 that IV piles moved separately because two neutral axes appeared. This behavior occurred when the interlocks slipped.

3.2.2 Case2: 45H-pile wall and IV-pile wall

Figure 16 shows the load–displacement curve of Case 2. When the load reached 1147 kN (358 kN/m for the IV-pile wall), the stress estimated from the strain on the flange of the IV pile at G.L$_{l.}$ = −1.5 m exceeded the standard yield stress, σ_y = 295 N/mm^2. Thereafter, the loading was completed. As shown in Figure 16, the gradient of the curve of the 45H-pile wall is considerably higher than that of the IV-pile wall.

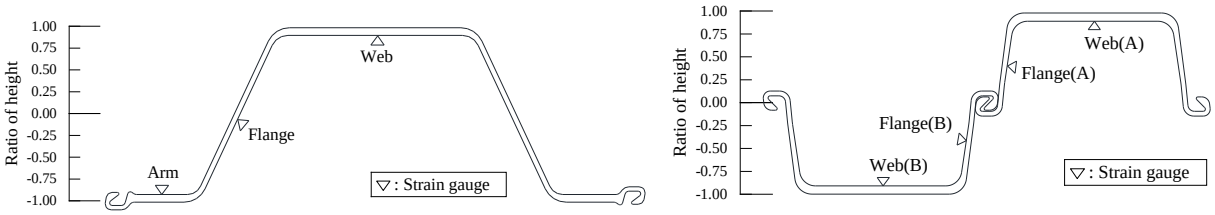

(a) 25H and 45H piles (b) IV pile

Figure 11 Sectional positions of strain gauges

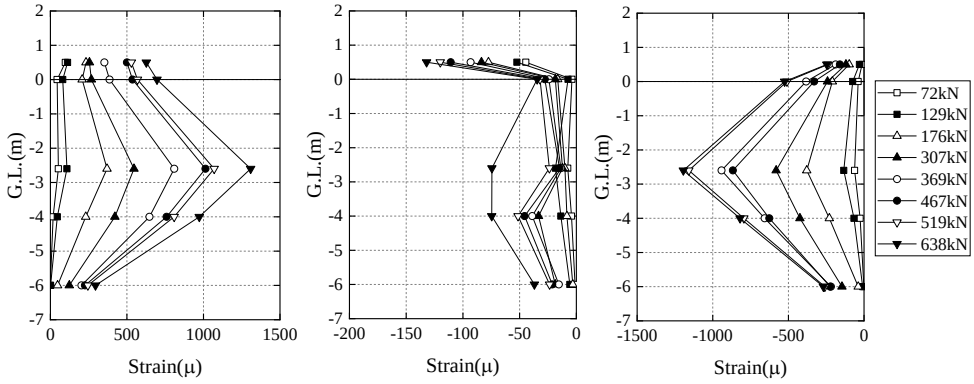

(a) Web (b) Flange (c) Arm

Figure 12 Strain distribution in the depth direction (25H-L16.5 pile)

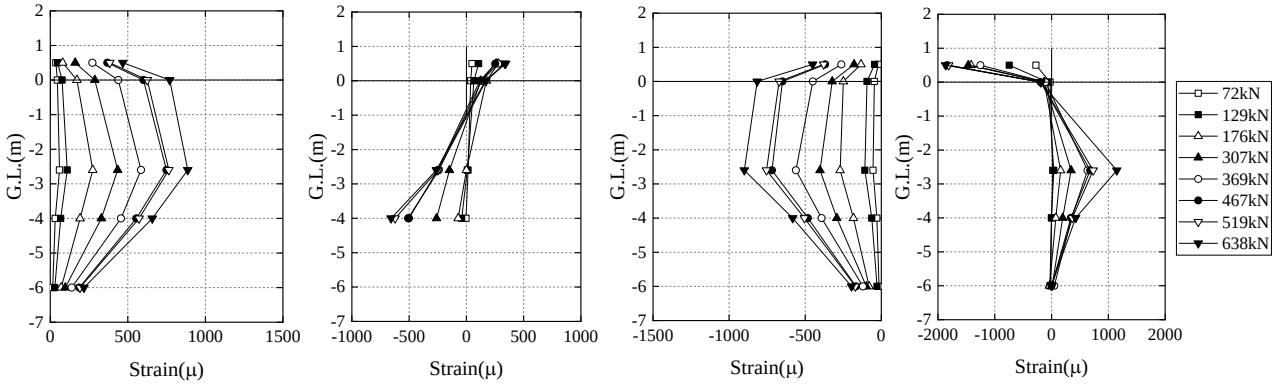

(a) Web (A) (b) Flange (A) (c) Web (B) (d) Flange (B)

Figure 13 Strain distribution in the depth direction (IV-L16.5 pile)

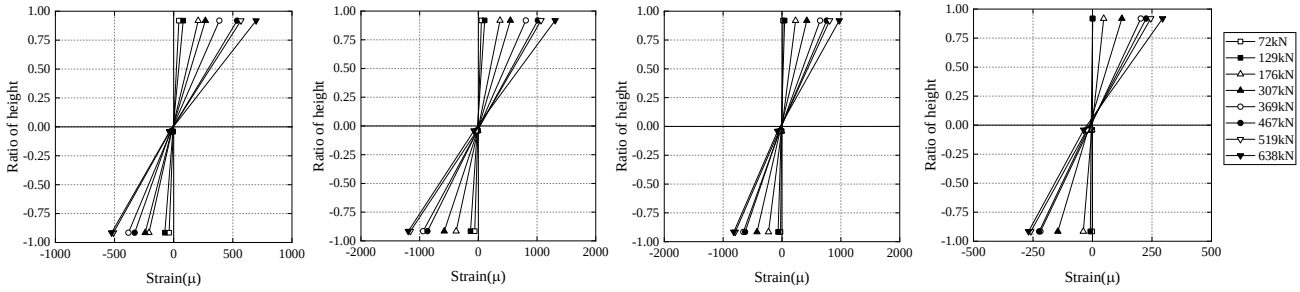

G.L. +0.0 m G.L. −2.6 m G.L. −4.0 m G.L. −6.0 m

Figure 14 Sectional strain distribution (25H-L16.5 pile)

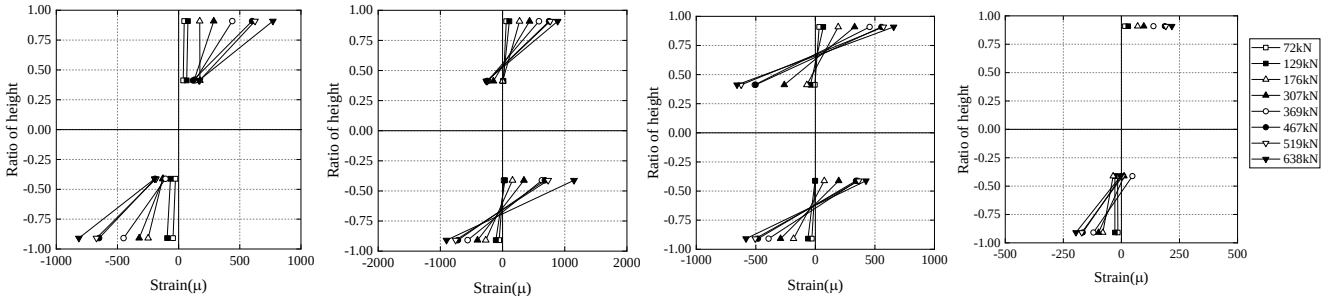

G.L. +0.0 m G.L. −2.6 m G.L. −4.0 m G.L. −6.0 m

Figure 15 Sectional strain distribution (IV-L16.5 pile)

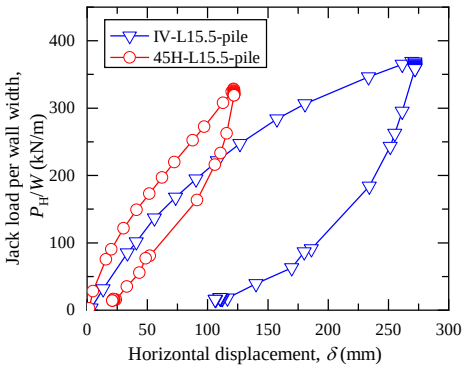

Figure 16 Relationship between the load per unit wall width and displacement in Case 2

Figures 17 and 18 show the strain distributions in the depth direction of each pile wall. As a result of changing the strain gauge levels, the actual maximum strains were probably obtained at approximately G.L$_1$. = −1.5 m. In the +45H-pile wall, strains on the web and arm portions were considerably higher than that on the flange portion. Conversely, in the IV-pile wall, the strain on the flange portion significantly increased after the load exceeded 962 kN.

These trends are similar to Case 1. As mentioned above, when the load reached 1147 kN, the maximum strain of 1550 μ at G.L$_1$. = −1.5 m, as shown in Figure 17(d), exceeded the standard yield strain. Figures 19 and 20 show the sectional strain distributions at each level. These are similar to that of Case 1, in which IV piles separately moved, whereas the 45H-pile wall performed as single wall. The IV piles exhibited this behavior when the interlock slipped.

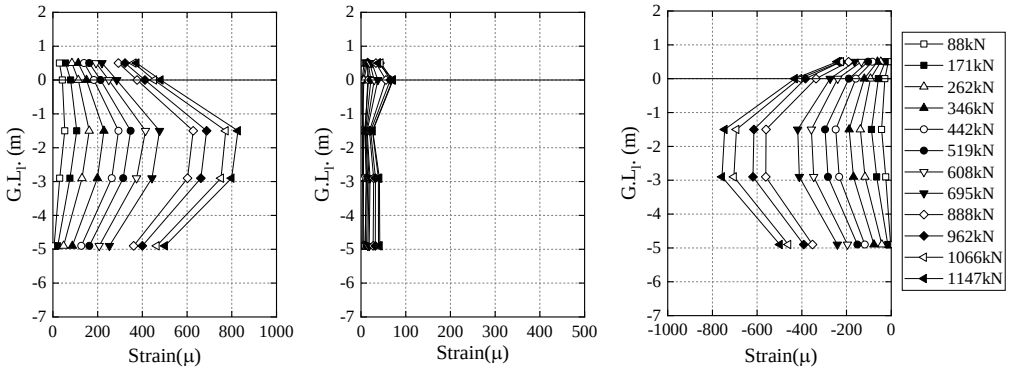

(a) Web (b) Flange (c) Arm

Figure 17 Strain distributions in the depth direction (45H-L15.5 pile)

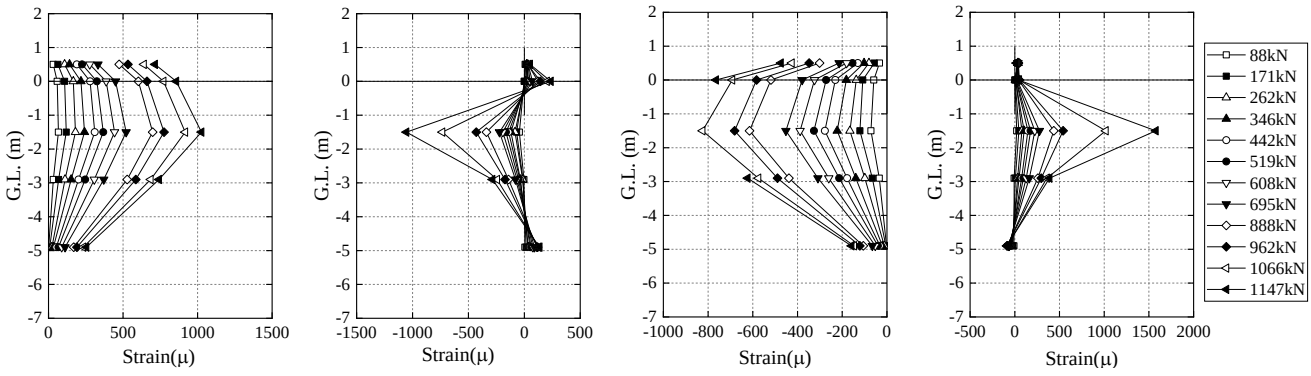

(a) Web (A) (b) Flange (A) (c) Web (B) (d) Flange (B)

Figure 18 Strain distributions in the depth direction (IV-L15.5 pile)

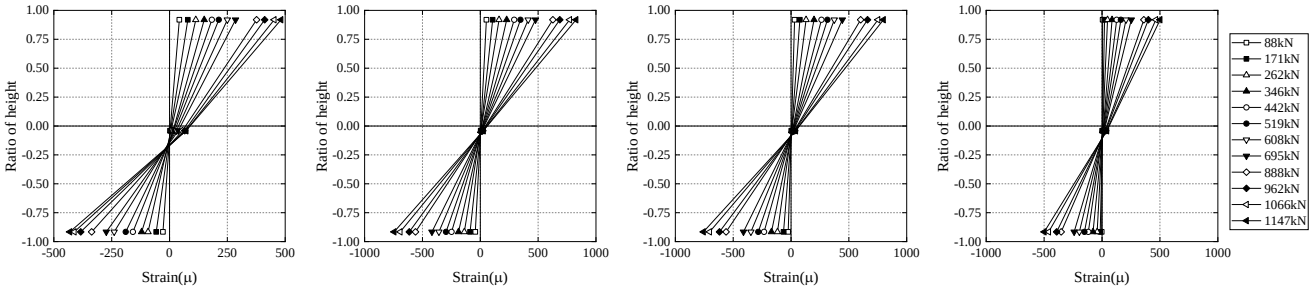

G.L. +0.0 m G.L. −1.5 m G.L. −2.9 m G.L. −4.9 m

Figure 19 Sectional strain distribution (45H-L15.5 pile)

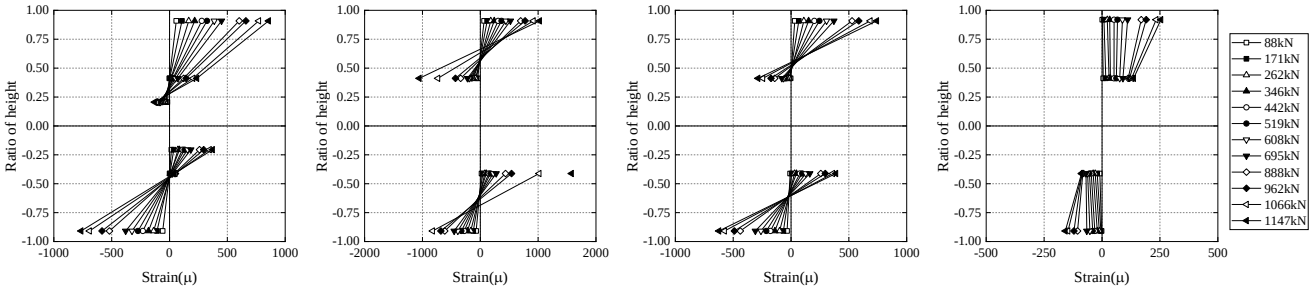

G.L. +0.0 m G.L. −1.5 m G.L. −2.9 m G.L. −4.9 m

Figure 20 Sectional strain distribution (IV-L15.5 pile)

3.3 Analysis of the shear force transmission at interlocks

3.3.1 Estimation based on the sectional strain distribution

The interlock slippage occurred in both cases of the IV-pile wall. In this section, the degree of the shear force transmission in the interlocks was estimated by means of two methods: analysis of the sectional strain distribution and load–displacement curve.

Figure 21 illustrates the sectional strain distribution related to the position of the neutral axis of the wall, where y_1 denotes the distance between the edge of the web side and neutral axis of a single pile; y_0 is the distance between the neutral axis of a single pile and edge of the interlock side; e is the distance between the neutral axis of a single pile and actual neutral axis of the pile wall. The actual sectional strain distribution depends on the transmission of the shear force, T, at the interlock. If T does not generate the slippage of interlocks, the neutral axis of the wall remains at the center of the wall ($e = y_0$), i.e., the full-shear transfer mode in Figure 21(a). In contrast, if T generates the full slippage of interlocks, the neutral axis of the wall corresponds to that of a single pile ($e = 0$), i.e., zero-shear transfer mode in Figure 21(b). When T generates the partial slippage of interlocks (i.e., partial-shear transfer mode in Figure 21 (c)), the neutral axis of the wall locates between that of the full and zero-shear transfer modes ($0 < e < y_0$).

Based on the study of Konoike (1986), the following shows the procedure in estimating the reduction factors, β_D and β_B, in relation to the location of the neutral axis of the wall. Here, β_D and β_B, denote the factors accounting for possible reductions in the moment of inertia and section modulus, respectively, because of the lack of shear force transmission at the interlocks. When the soil pressure generates the bending moment, M, on the pile wall, the stress, σ_y, at a distance, y, from the neutral axis of a single pile is

$$\sigma_y = \frac{(M - 2Ty_0)}{I_1} y - \frac{2T}{A} \tag{1}$$

where I_1 and A denote the moment of inertia and sectional area of a single pile, respectively.

Because the stress, σ_y, is zero at the center of the wall ($y = e$)

$$\frac{(M-2Ty_0)}{I_1} e = \frac{2T}{A} \tag{2}$$

Then, the shear force, T, is

$$T = \frac{eAM}{2(I_1 + y_0 eA)} \tag{3}$$

Next, the stress, σ_w, at the web is

$$\sigma_w = \frac{M - 2Ty_0}{I_1}(-y_1) - \frac{2T}{A} \tag{4}$$

From Eqs. (3) and (4), the stress, σ_w, appears as

$$\sigma_w = -\frac{M}{I_1 + y_0 eA}(y_1 + e) \tag{5}$$

Thus, the moment of inertia, I, can be described as

$$I = I_1 + y_0 eA \tag{6}$$

Moreover, the section modulus, z_w, at the edge of the sheet pile web is

$$z_w = \frac{I_1 + y_0 eA}{y_1 + e} \tag{7}$$

The stress, σ_t, at the interlock is obtained from Eqs. (1) ($y = y_0$) and (3):

$$\sigma_t = -\frac{M}{I_1 + y_0 eA}(y_0 - e) \tag{8}$$

Thus, the section modulus, z_t, at the interlock is

$$z_t = \frac{I_1 + y_0 eA}{y_0 - e} \tag{9}$$

In the full-shear transfer mode, the neutral axis of the wall is located at the center of the wall ($e = y_0$). Then, the stress, σ_{w0}, section modulus, z_{w0}, at the web, and moment of inertia are

$$\sigma_{w0} = -\frac{M}{I_1 + Ay_0^{\,2}}(y_1 + y_0) \tag{10}$$

$$z_{w0} = \frac{I_1 + Ay_0^{\,2}}{y_1 + y_0} \tag{11}$$

$$I_0 = I_1 + Ay_0^{\,2} \tag{12}$$

Thus, β_D is defined as

$$\beta_D = \frac{I}{I_0} = \frac{I_1 + y_0 eA}{I_1 + Ay_0^{\,2}} \tag{13}$$

As for β_B, there are two equations involved, i.e., β_w at the web and β_t at the interlock:

$$\beta_w = \frac{Z_w}{Z_{w0}} = \frac{y_0 + y_1}{y_1 + e} \times \frac{I_1 + y_0 eA}{I_1 + Ay_0^{\,2}} = \frac{y_0 + y_1}{y_1 + e}\beta_D \tag{14}$$

$$\beta_t = \frac{Z_t}{Z_{w0}} = \frac{y_0 + y_1}{y_1 - e} \times \frac{I_1 + y_0 eA}{I_1 + Ay_0^{\,2}} = \frac{y_0 + y_1}{y_0 - e}\beta_D \tag{15}$$

It is assumed that the section modulus on the side generated the maximum stress.

The maximum stress is generated at the edge of the web when $e > \frac{y_0 - y_1}{2}$, whereas it is generated at the interlock under the condition $e < \frac{y_0 - y_1}{2}$.

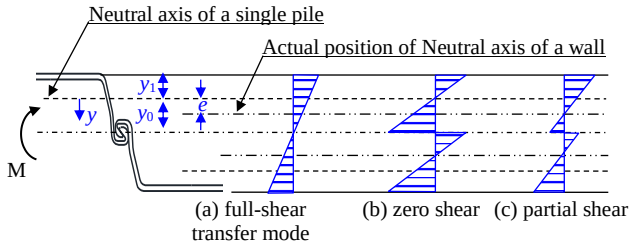

Figure 21 Relationship between the neutral axis position and shear transfer mode

Figure 22 shows the theoretical values of β_D, β_t, and β_w in relation to the position of the neutral axis in the case of the IV-pile wall. When the neutral axis of the pile wall is located at the center of the wall ($e = y_0$), the wall behaves as a single wall. When the neutral axis of the pile wall shifts from the center of the wall to the location of the neutral axis of a single pile, β_D decreases linearly with decreasing e. The cross point of β_w and β_t at $(y_0 - e)/(y_0 + y_1) = 0.5$ means the maximum stress side changes from the web side to the interlock side. After the neutral axis exceeds half of the effective sheet pile height ($e < (y_0 - y_1)/2$), β_B rapidly decreases, whereas the maximum stress at the interlock rapidly increases. Each factor reaches the minimum value when the neutral axis of the pile wall is located at the same position as that of a single pile.

In Cases 1 and 2, β_D of the IV-pile wall was estimated based on the actual neutral axis position shown in Figures 15 and 20 by using Eqs. (13)–(15). Figures 23 and 24 show the relationship between the jack load and β_D. These figures indicate that the interlock of the IV-pile wall slipped because β_D was less than the value of that in the full-shear transfer mode ($\beta_D = 1.0$). This is true except at G.L. 0 m, under the small jack load in Case 1 and at G.L. −4.9 m in Case 2. In detail, the relationships between β_D and jack load of Case 1 differed from those in Case 2. In Case 2 (Figure 24), β_D at each level practically remained the same without exhibiting any relationship with the jack load. However, in Case 1 (Figure 23), β_D decreased with the increase in the jack load from 72 kN to 369kN. When the load exceeded 369kN, β_D kept almost constant. The difference between Case 1 and Case 2 may be caused by the difference of the piling situations. When the pile was installed at L_e = 15.0 m in the piling in Case 1, one of the interlocks melted partially because of the excess frictional heat generated by pile-driving vibrations. After the heat was cooled, the partially melted interlock was deposited. Therefore, such a crimped condition was generated partially in the interlock. Because this deposited portion of the interlock may be separated gradually with increase in the load in Case 1, β_D decreased gradually. The deposited portion of the interlock was separated perfectly at P_H = 369kN. Then, β_D converged to a constant value. Regarding Case 2, such a melting of the interlock was not observed during the piling. Therefore, the interlocks were separated and slipped from the beginning of the loading.

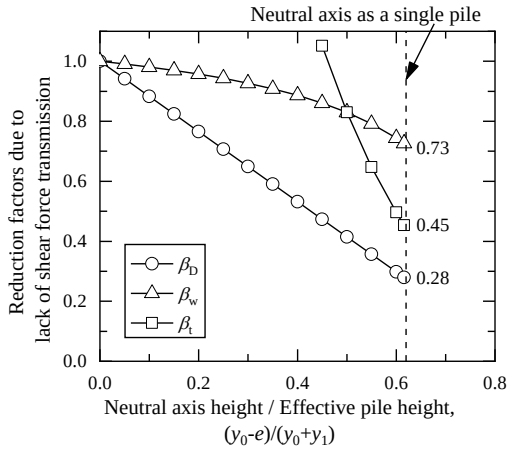

Figure 22 Theoretical Relationship between the position of the neutral axis of IV-pile wall and reduction factors

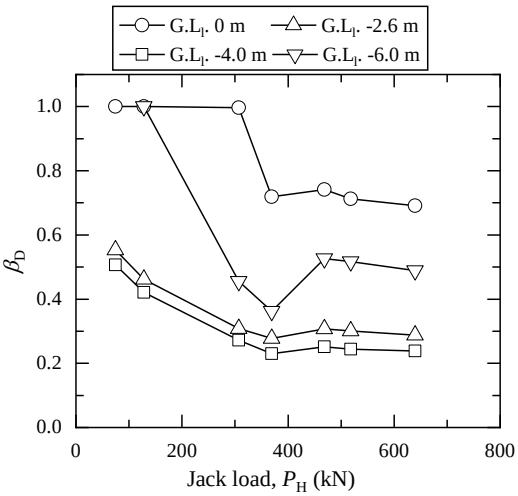

Figure 23 Relationship between the jack load and β_D of IV-L16.5 pile in Case 1

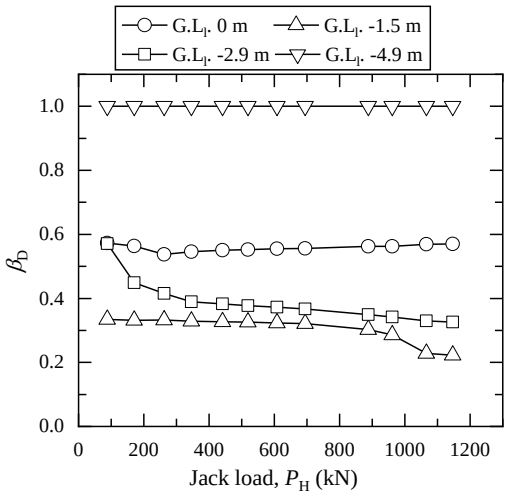

Figure 24 Relationship between the jack load and β_D of IV-L15.5 pile in Case 2

Figures 25 and 26 show the relationship between the jack load and β_B. When β_B drops below 0.82, which is the cross point shown in Figure 21, the maximum stress side changes from the web side to the interlock side.

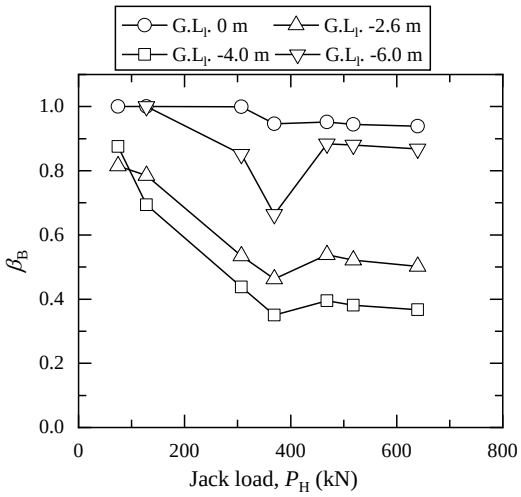

Figure 25 Relationship between the jack load and β_B of IV-L16.5 pile in Case 1

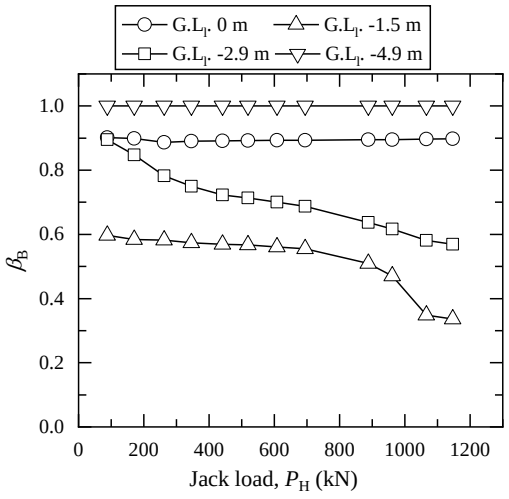

Figure 26 Relationship between the jack load and β_B of IV-L15.5 pile in Case 2

It can be observed from Figures 25 and 26 that the maximum stress on the IV-pile was generated at the interlock side at G.L. −2.6 m and G.L. −4.0 m wall in Case 1, and at G.L. −1.5 m and G.L. −2.9 m in Case 2. As explained above, β_D and β_B can be estimated from the sectional strain distribution at each level, noting that these factors differed at each level. In the following section, the overall flexural stiffness of the pile (i.e., the overall β_D for the pile wall) was estimated using another method.

3.3.2 Estimation based on the load–displacement curve relationship

In this section, β_D is estimated from the load–displacement curve using Chang's formation. This approach premises that the interlock of the Hat-pile wall remains under the full-shear transfer mode, because its neutral axis did not move during the load test, as shown in Figures 14 and 18. The coefficient of the subgrade reaction, k_h, can then be calculated from Chang's formula:

$$\delta_P = \frac{(1+\beta h)^3 + 1/2}{3EI\beta^3} P_H \tag{16}$$

$$\beta = \sqrt[4]{\frac{k_h B}{4EI}} \tag{17}$$

where P_H, δ_P, I, E, β, and W denote the jack load, horizontal displacement of the sheet pile, moment of inertia of the sheet pile, Young's modulus, characteristic value of a pile, and sheet pile wall width, respectively.

The unknown factor, k_h, is obtained from Eqs. (16) and (17), because other factors of the Hat-pile wall are known, including the P_H–δ_P relationship obtained by the load test. As shown in Figure 27, the calculated value of k_h decreased significantly and converged with increasing P_H.

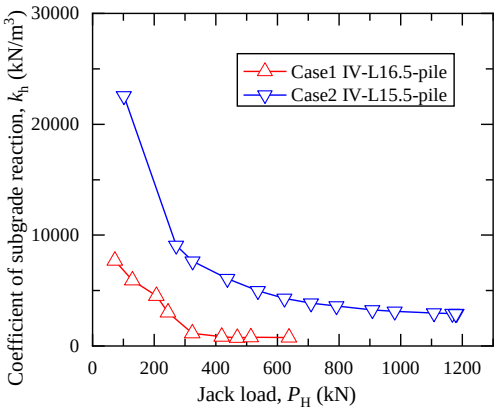

Figure 27 Estimated coefficient subgrade reaction, k_h

Next, the P_H–δ_P chart corresponding to various values of I can be estimated by using Eqs. (16) and (17), and k_h. Figures 28 and 29 show the comparison between the P_H–δ_P chart and test results of the IV-pile wall for each case. Here, β_D = 1.0 means that the estimated P_H–δ_P relationship is under the full-shear transmission mode of the IV-pile wall (i.e., I = 38 600 cm^4/m as listed in Table 4). As shown in both figures, β_D of the IV-pile wall can be read as 0.3 during the initial loading stage. Thereafter, β_D increases to 0.4 during the medium loading stage. Finally, β_D decreases to the same value of 0.3 or less.

4. EXCAVATION TEST

4.1 Test method

The lateral load test clarified that the interlock in the IV-pile wall slipped, and β_D was 0.3–0.4. However, the test condition relates to a particular situation, where the ground at the rear and that at the front

of the pile wall were at the same level, and the top of the wall was pushed by the jack. In order to verify the flexural stiffness, including the interlock slippage in an actual situation, an excavation test was performed.

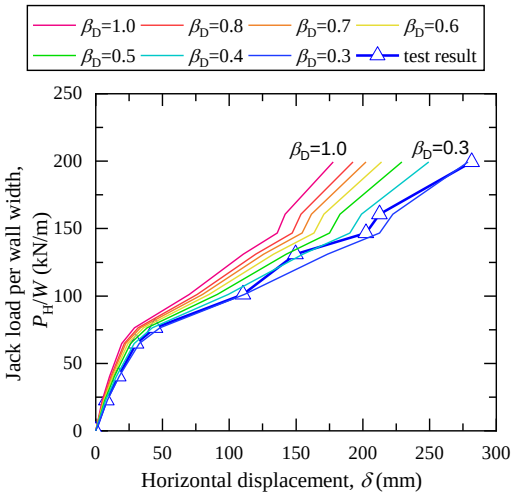

Figure 28 Relationship between the β_D chart and load–displacement of the IV-L16.5 pile wall in Case 1

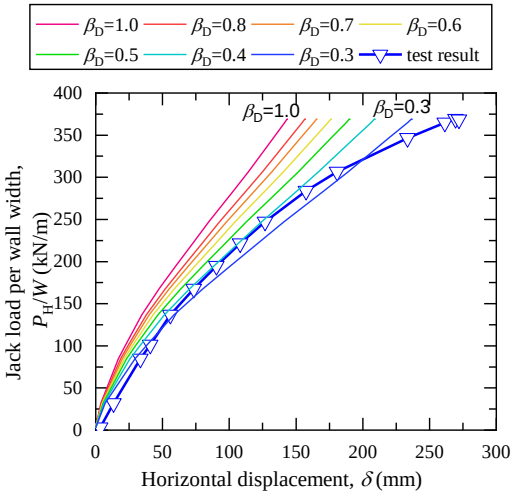

Figure 29 Relationship between the β_D chart and load–displacement of the IV-L15.5 pile wall in Case 2

As listed in Table 1, two cases were carried out in the excavation test. The flexural stiffness of the 25H-pile wall was compared with that of the IV-pile wall in Case 3, whereas the 45H-pile wall was compared with the IV-pile wall in Case 4. Figure 5 illustrates the relationship between the soil condition and pile embedment length, L_e. After the construction of the cofferdam, sand was backfilled 0.6 m from the upper ground surface for the lateral load test. In this section, the new backfilled ground is defined as ground surface, G.L$_e$. The 25H-pile wall and the IV-pile wall in Case 3 have L_e = 11.1 m, whereas the 45H- pile wall and the IV-pile wall in Case 4 have L_e = 14.6 m. All of the piles in the excavation test were reused from the aforementioned lateral load test. Figure 3 shows the construction procedure of the cofferdam for the excavation test. In the process of the construction, the upside of IV piles for Case 3 was cut to remove the residual bent by the lateral load test. The length of the piles was reduced from 16.5 to 12 m. The 25H piles were cut to fit the length of IV piles too. On the other hand, the piles in Case 4 were used continuously from the lateral load test. Therefore, these piles had residual displacements caused by the lateral load test. The residual displacements in the 45H-pile and IV-pile walls were 22 and 106 mm, respectively. The influence of residual displacement is discussed in the next section. The side wall of the cofferdam was constructed using Hat piles.

As shown in Figure 30, an excavator dug the inside of the cofferdam. In order to measure the displacement of the pile wall, displacement transducers were set at a point 370 mm below the top of each pile. Figure 31 shows the transducer locations. When the excavated depth reached G.L$_e$. = −5.8 m, the horizontal displacement of the IV-L12-pile wall exceeded 100 mm, and excavation was stopped at that point. After a 17-h rest period, measurements of horizontal displacements were repeated. This completed the excavation test.

Figure 30 Cofferdam excavation

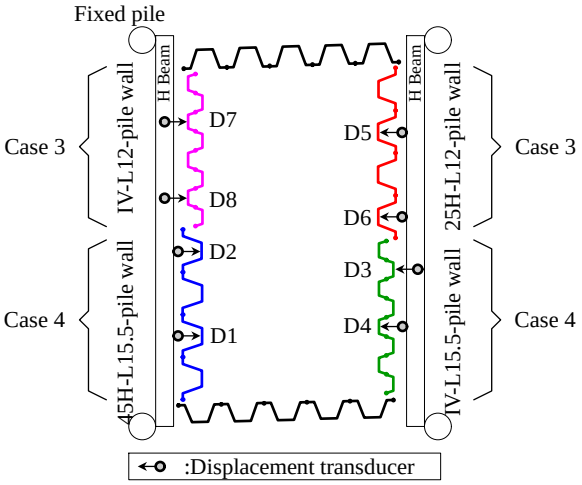

Figure 31 Measuring points of sheet pile displacement

4.2 Test result

Figure 32 shows the relationships between the excavated depths and horizontal displacements of the pile walls. The original point on the vertical axis of the graph indicates the vertical line from the ground. The displacements of the IV-L12-pile and 25H-L12-pile walls in Case 3 (D1–D4 in Figure 32) started from the original point, because these piles were reinstalled vertically to the ground. Conversely, the displacements of the IV-L16-pile and 45H-L16-pile walls in Case 4 (D5–D8 in Figure 32) started from the negative value, because the residual displacements to the side opposite of the excavated side were generated by the previous lateral load test as mentioned in the above section.

As shown in Figure 32, horizontal displacements of the pile walls relatively increased after the excavation depth exceeded 2 m. Among the walls, the IV-L12-pile wall exhibited the maximum displacement. It is remarkable that the displacement of the 25H-L12-pile wall was 45% smaller than that of the IV-L12-pile wall, although the moment of inertia of a single 25H pile is 37% lower than that of a single IV

pile, as listed in Table 4. The reason for this is that the flexural stiffness of the IV-pile wall decreased because of the lack of interlock integrity.

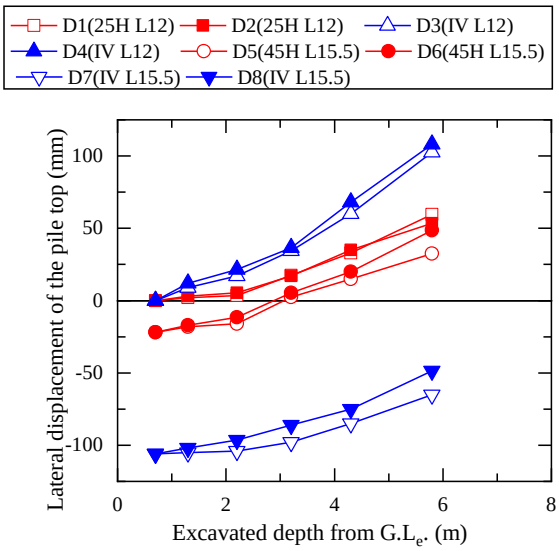

Figure 32 Relationship between the excavated depth and lateral displacements

In order to evaluate the results of the IV-L15.5-pile and 45H-L15.5-pile walls in Case 4, the residual displacement of the previous lateral load test must be considered. As shown in Figure 33, in the lateral load test, the IV-L15.5-pile wall was displaced to the opposite side of the excavated ground with a magnitude larger than that sustained by the 45H-L15.5-pile wall. Hence, the initial displacement of the IV-L15.5-pile wall was smaller than that of the 45H-L15.5-pile wall (45H: −22 mm, IV: −106 mm). Furthermore, in the lateral load test, the counter side of the excavated ground of the IV-L15.5-pile wall was compressed higher than the 45H-L15.5-pile wall was. Therefore, in the excavation test, the active earth pressure and elastic rebound acting on the IV-L15.5-pile wall probably became smaller than that acting on the 45H-L15.5-pile wall, as illustrated in Figure 33. In addition, the degree of the elastic rebound of the 45H pile itself was higher than that of the IV pile, because the 45H pile remained in the elastic condition, whereas the IV pile reached the plastic condition in the lateral load test. In relation to the lateral load test, these influences should be considered to appropriately evaluate behaviors of the 45H-L15.5-pile and IV-L15.5-pile walls.

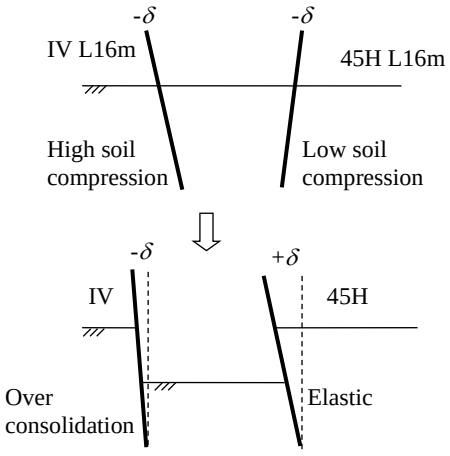

Figure 33 Change in the soil condition from the lateral load test to the excavation test

4.3 Back analysis to estimate the lack of shear force transmission

To estimate the actual flexural stiffness of IV-piles in the excavation test, a back analysis was performed using a finite element analysis application, PLAXIS (version 2016.01). The analysis premise is that the interlock of the 25H-12L pile maintained the full-shear transfer mode (β_D = 1.0) based on the result of the lateral load test. On the other hand, β_D of IV-piles were sought to fit the pile top lateral displacement of the excavation test, because the test showed a lack of interlock integrity as mentioned above. The purpose of this analysis is to find the magnitude of the lack of interlock integrity, β_D, of IV-piles.

Figure 34 shows the overview of the PLAXIS mesh model. In the analysis, after the pile walls were set in the original ground, the soil within the walls was gradually removed to a final depth of G.L$_e$. = −5.8 m. Table 5 summarizes the soil parameters. All soil materials were modeled with the Mohr-Coulomb model. As shown in the table, the parameters were classified into the original soil parameters, designed soil parameters, or estimated soil parameters. First, the original parameters (i.e., unit weight, γ, and undrained cohesion, c_u of the L2 to L4 layers) were obtained by the soil investigation. The undrained cohesions, c_u, of layers L2 and L3 were investigated by means of the unconfined compression test, and c_u of L4 was measured by the direct shear test. Next, the designed soil parameters had the general design value or were decided based on Land Transport Authority (2010). Regarding the L1 layer, c_u and the effective friction angles, ϕ', were taken from the design parameters for the fill layer in Land Transport Authority (2010). The modulus of elasticity, E, is a general design value for a fill layer in Singapore. In all layer, Poisson's ratio, ν, was 0.3, because the value is general in this kind of simulation. Finally, other parameters were estimated considering the excavation test situation. Because the rest time of the excavation test, 16-h, was short for the clay layer of L2 to L4, an undrained condition was selected. Therefore, ϕ' of these layers was zero. On the other hand, the water permeability of the L1 layer was higher than that of the L2 to L4 layer, because the water table was located in the L1 layer, and the cobbles were included in the upper section of the layer. Therefore, the L1 layer was treated as a drained condition. Furthermore, γ of L1 and E of L2 to L4 were adjusted to represent the soil pressures at the time. Compared with the design parameters, a smaller γ and higher E were used, i.e., γ = 19 kN/m^3 for the fill layer based on Land Transport Authority (2010), and E = 0.3 c_u is a general design value in Singapore. The reason for the difference between the estimated value and the design value is the rest time. If the rest time were longer, the estimated values would be changed from the values listed in Table 5. Actually, the displacement was increased approximately 20 mm over a 16-h period. Hence, if the target were the final value of the displacement, the soil parameters would have to be closer to the design parameters. Regarding the L5 layer, c_u and E were set relatively lower than those of the L2 to L4 layers, because the SPT N value of the L5 layer was lower than that of these layers. The soil parameters of the L5 layer had little influence on the deformation, because the layer was deeper than the pile tip depth.

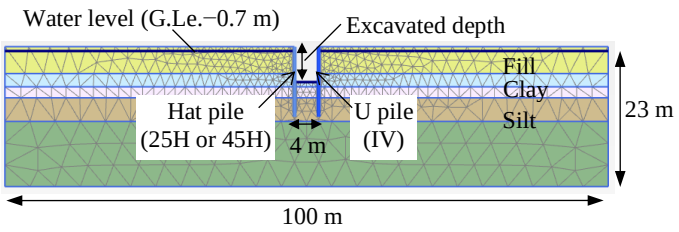

Figure 34 Overview of the PLAXIS excavation simulation model

Table 5 Soil parameters of the back analysis for the excavation test

Layer No.	Thickness	G.Le.	Soil Class.	Unit Weight	Deformation Modulus	Undrained Cohesion	Effective friction angle	Poisson's ratio	Coefficient of Earth Pressure
				γ	E	c_u	ϕ'	ν	k_o
	m	m	-	kN/m^3	kN/m^2	kN/m^2	deg.	-	-
L1	4.4	0 ~ -4.4	Fill	15.2$^+$	10000$^\#$	0.5$^\#$	30.0$^\#$	0.3$^\#$	0.5
L2	2.2	-4.4 ~ -6.6	Clay	15.1*	54200$^+$	45.2*	0$^+$	0.3$^\#$	1.0
L3	1.8	-6.6 ~ -8.4	Clay	16.1*	46000$^+$	38.3*	0$^+$	0.3$^\#$	1.0
L4	3.9	-8.4 ~ -12.3	Silt	19.1*	31200$^+$	26.0*	0$^+$	0.3$^\#$	1.0
L5	10.7	-12.3 ~ -23.0	Silt	20.0$^+$	24000$^+$	20$^+$	0$^+$	0.3$^\#$	1.0

*: Original soil parameters measured by the soil investigation

#: Designed soil parameters were general design value or decided based on Land Transport Authority (2010)

+: Estimated soil parameters considering the excavation test situation.

The sheet piles were modeled with the elastic beam model. The dimensional properties shown in Table 3 were used for all piles. Young's modulus of all piles was 205800 kN/m^3. The moment of inertia, *I*, of the 25H-pile and 45H-pile were the values shown in Table 4, because Hat-piles were verified to perform the full-shear transfer mode (β_D = 1.0). On the other hand, *I* of the IV-pile was unknown, and it was presumed to be smaller than that of the 25-pile, because the lateral displacement of the pile top of IV-L12-pile was larger than that of the 25H-L12-pile. Therefore, in the simulation, *I* of the IV-pile was varied to fit the test result.

As a result, when β_D of the IV-12L-pile wall was 0.4, the PLAXIS results agreed with test results. Figure 35 compares the results of PLAXIS with those of the test. The PLAXIS results corresponded to the test results. This means that the flexural stiffness of the IV-12L-pile wall decreased because of the interlock slippage (β_D = 0.4). Moreover, the line of the 45H-12L-pile wall in Figure 35 shows the result of the simulation (β_D = 1.0).

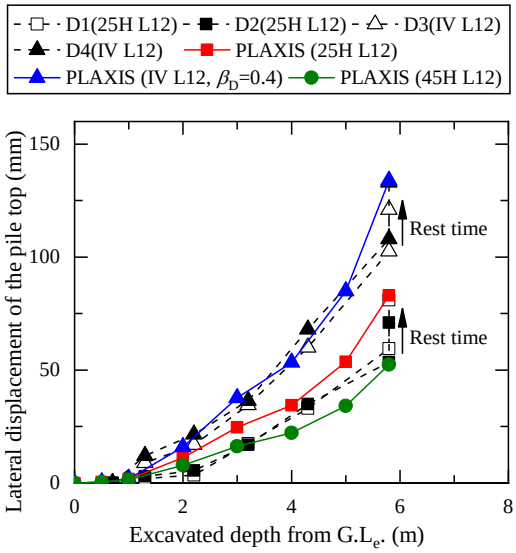

Figure 35 Comparison between PLAXIS and test results

As mentioned above, in the excavation test, the residual deformation from the lateral load test makes it difficult to appropriately evaluate the performance of the 45H-pile wall. As shown in Figure 35, it is clear that the displacement of the 45H-pile wall is the smallest because of its higher stiffness.

5. CONCLUSIONS

In order to verify and compare the flexural stiffness, including the difference of the interlock shear force transmission between the Hat-pile and U-pile walls, a series of field tests was performed in Singapore. The findings are as follows:

1) In the lateral load test, the 25H-pile wall exhibits a flexural stiffness that is the same or higher than that of the IV-pile wall, although the moment of inertia, *I*, of the single IV pile is one-half that of the 25H pile. The reason for this is the inefficiency of the shear force transmission on the IV-pile wall. The sectional strain distribution of the IV-pile wall clearly verified the separate movement of the piles in the wall. In contrast, the sectional strain distribution of the 25H-pile wall maintained the neutral axis at the center of the wall. This is the reason that Hat-type sheet piles can perform full-shear force transmission.
2) The excavation test was conducted to compare the flexural stiffness of the walls in an actual situation. The comparison showed that the horizontal displacement of the 25H-pile wall was smaller than that of the IV-pile wall. Similar to 1), the result verified that the 25H-pile wall can achieve a higher flexural stiffness than the IV-pile wall.
3) The degree of insufficiency of the shear force transmission in the IV-pile wall was estimated in three ways: estimation from the sectional strain distribution, P_h–δ relationship in the lateral load test, and back analysis of the excavation test. As a result, β_D, the factor accounting for the possible reduction in the moment of inertia because of the lack of shear force transmission in the interlocks, was estimated to be 0.3–0.4 by means of these methods.

This study verified that the IV-pile wall, as a cantilever, has β_D = 0.3–0.4. This β_D corresponds to the value described in EN 1993-5, i.e., under the condition of no crimp and no strut, β_D = 0.3 for highly unfavorable soil conditions, β_D = 0.35 for unfavorable soil conditions, and β_D = 0.40 for favorable soil conditions. The soil condition of the test field may be classified as an unfavorable soil condition. In contrast, the Hat-type sheet piles, such as the 25H and 45H piles do not need to have their flexural stiffness reduced, because the series of field tests, particularly the sectional strain distribution, verified that the Hat-pile wall can behave as a single wall. This difference between Hat piles and U piles influences productivity.

Figure 36 shows the relationship between the unit mass and moment of inertia per meter width of wall of both pile types. When β_D of the IV-pile wall was 0.4, its moment of inertia significantly decreased from that when β_D = 1.0. Conversely, it does not need to consider the insufficiency of the shear force transmission in the 25H-pile wall. Thus, the moment of inertia of the 25H-pile wall is superior to that of the IV-pile wall. Additionally, the plot of β_D = 0.55 in the figure is the maximum value for the uncrimped pile wall with struts in EN 1993-5.

Accordingly, the Hat-pile wall exhibits superior flexural stiffness per unit mass compared to the U-pile wall. Although β_D can be increased by crimping or welding at the interlock, these can make the productivity worse. As described above, the Hat-pile wall can improve the steel unit weight per meter width of wall and achieve a reasonable sheet pile wall design. Furthermore, the Hat pile can reduce the number of piles and piling time for the wall because of its wide width. Therefore, the Hat pile can significantly contribute to the

improvement of productivity, construction technology, and economic efficiency.

Moreover, a Hat pile can expand its high flexural stiffness zone by combining it with an H beam. As Matsui (2015) mentioned, the Hat + H pile, composed of a Hat pile with an H beam has a high flexural stiffness, which is the same as or higher than that of a secant pile wall and built-up U-pile with an H beam (i.e., solder pile). Therefore, the Hat pile has the potential of improving productivity in the wider flexural stiffness zone.

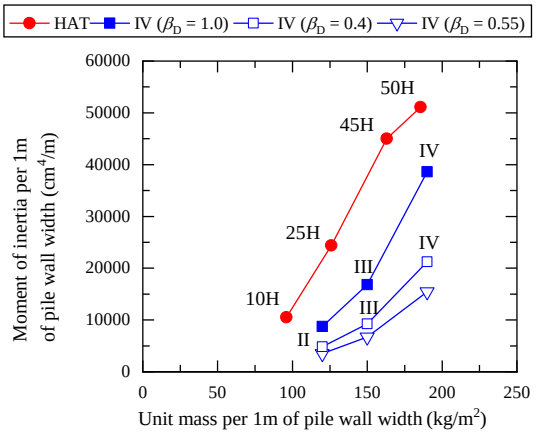

Figure 36 Comparison of moments of inertia including β_D between Hat and U piles

6. ACKNOWLEDGEMENT

The authors would like to express their thanks to their field test partners: Antara Koh Pte. Ltd., Kiso-Jiban Singapore Pte. Ltd., Avenue Engineering Pte. Ltd., and Keisoku Soft Co.Jp. Moreover, the authors acknowledge the support of the staff of the Singapore Institute of technology, Mr. Higuchi, Ms. Ma. Charisse B. Macaraeg, Ms. Shang Yi Chang, and other members of the Nippon Steel & Sumitomo Metal corp., Mr. Eka Pradana Susanto, PT. Nippon Steel, and Sumitomo Metal Indonesia.

7. REFERENCES

Building and Construction Authority (2012) "Design Guide on Use of Alternative Structural Steel to BS 5950 and Eurocode 3.

Byfield, M.P., Mawer, R.W., (2004) "Analysis of reduced modulus action in U-section steel sheet piles", Journal of Constructional Steel Research, 60, pp401-410.

EN1993-5 “Eurocode 3 Design of steel structures”.

Crawford, R.J., Byfield, M.P., (2002) "A numerical model for predicting the bending strength of Larssen steel sheet piles", Journal of Constructional Steel Research, 58, pp1361-1374.

Endley, Snow, Knuckey, Briaud and Lowery, (2000) "Performance of an anchored sheet pile wall", Geotechnical Mesurements ,106, pp179-197.

Harata, N., Tatsuta, M., Kurosawa, T., Nishiumi, K., et al (2008) "Development of Hat-type Sheet Pile 900", Nippon Steel Technical Report, 97, pp11-18.

JIS A 5523 (2012) "Weldable hot rolled steel sheet piles".

Otsushi, K., Harata, N., Nishiyama, T., Yamashita, H., Miura, Y., et al (2016) "Line-up Expansion of Hat-shaped Steel Sheet Pile (NS-SP-45H, 50H) ", Nippon Steel & Sumitomo Metal Technical Report, 113, pp57-63.

Konoike, K., (1986) "Experimental study on section rigidity of steel sheet-pile wall", Journal of Japan Society of Civil Engineers, 373, pp74-83.

Land Transport Authority (2010) "Civil Design Criteria for Road and Rail Transit Systems".

Matsui, N., Eka, S., Teshima, K., Akahoshi, T., Terasaki, S., et al (2015) " Novel Compound Steel Sheet Pile for Earth Retaining Works", The IES Journal Part A: Civil & Structural Engineering.

Shiraishi, M., (1987) "Theoretical analysis of U-type sheet pile wall on shearing resistance force of interlocking joints and sectional properties, 385, pp49-58.

Singapore National Annex to Eurocode 3 : Design of steel structures – Part 5: Piling (2010) .

UK National Annex to Eurocode 3 : Design of steel structures – Part 5: Piling (2007).